Accessing Ni(0) to Ni(IV) via Nickel-Carbon-Phosphorus Bond Reorganization

Journal:	*ChemComm*
Manuscript ID	CC-COM-09-2023-004687.R1
Article Type:	Communication

SCHOLARONE™
Manuscripts

COMMUNICATION

Accessing Ni(0) to Ni(IV) via Nickel-Carbon-Phosphorus Bond Reorganization

Lirong Lin,[a] David S. Tresp,[a] Denis M. Spasyuk,[b] Roger A. Lalancette,[a] and Demyan E. Prokopchuk[a]*

0000-0002-2883-2349 (LL); 0000-0003-4743-6269 (DST); 0000-0001-9018-3063 (DMS);

0000-0002-3470-532X (RAL); 0000-0002-6352-3509 (DEP)

Two-electron oxidation of a Ni[II]Ph(PCP) pincer complex initiaites phosphine ligand insertion, generating an η^6-arylphosponium moiety coordinated to Ni[II]. The reaction is fully reversible under reducing conditions. X-ray crystallography, NMR/EPR spectroscopy, electrochemistry, and DFT calculations support the proposed Ni-C-P bond reorganization mechanisms, which access oxidation states from Ni[0] to Ni[IV].

Organophosphines (PR_3) are ubiquitous ancillary ligands, prized for their nearly limitless synthetic, steric, electronic, and structural modularity in homogeneous catalysis. However, PR_3 ligands relinquish their ancillary role during the Ni- or Pd-catalyzed synthesis of arylphosphonium salts according to the following general equation: $PAr_3 + Ar'X \rightarrow [Ar'PAr_3][X]$.[1-5] Early mechanistic work by Kochi showed that Ni[I] and Ni[III] complexes can both facilitate P-C bond formation;[6] based on these findings, others have proposed mechanisms involving Ni[I/III] redox cycling, where $[Ni^{III}(Ar')(PAr_3)_2(L)]^{2+}$ or $Ni^{III}X_2(Ar')(PAr_3)(L)$ release $[Ar'PAr_3]^+$ via reductive elimination, generating a Ni[I] intermediate which subsequently reacts with Ar'X via oxidative addition.[1, 3]

In contrast to the chemically active role of PR_3 ligands described above, incorporating organophosphines into thermally and chemically robust tridentate pincer frameworks enables them to persist as ancillary ligands throughout catalysis. Notably, nickel complexes containing PCP ligands can catalyze H_2 production,[7] the hydroamination of acrylonitrile,[8] and the fluorination of benzyl halides.[9] Our group is interested in understanding the fundamental reactivity of group 10 complexes containing a lesser-known class of adamantyl-derived PCP pincer ligands,[10-12] as shown in Scheme 1. We recently found that the central alkyl moiety of **PCPNiBr** can be protonated to yield an agostic CH_2 moiety, enabling us to quantify its

coordination-induced $C(sp^3)$-H bond weakening via pK_a measurements and electrochemical analysis of the Ni[III/II] redox couple.[13] Herein, we describe an unprecedented instance of oxidatively triggered aryl insertion into the pincer phosphine atom of **1**, generating arylphosphonium salt **2** that retains its coordination to nickel through an η^6-arene bond. Remarkably, this reaction is reversible – the newly formed P-C bond collapses under cathodic conditions to regenerate **1** through a Ni[0] (η^6-arene) intermediate, as supported by electrochemical measurements and DFT calculations. These redox-controlled nickel-carbon-phosphorus bond reorganization reactions provide insights into the broad range of accessible oxidation states (Ni[0] to Ni[IV]) using adamantyl-based PCP pincer ligands and highlight the possible role of η^6-arene interactions during nickel-catalyzed arylphosphonium synthesis.
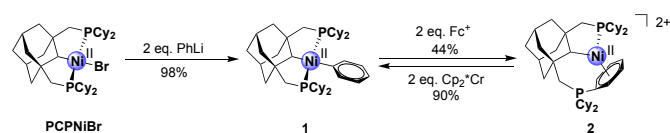
Scheme 1. Synthesis of complex **1** and complex **2**.

Treatment of **PCPNiBr** with excess phenyllithium at -40 °C affords the complex **PCPNiPh** (**1**) in 98% yield after workup (Scheme 2). The ^{31}P NMR spectrum in C_6D_6 reveals a singlet at 48.8 ppm, which is nearly identical to the chemical shift of **PCPNiBr** (49.0 ppm).[13] The Ni-CH$_{alkyl}$ NMR spectral resonances appear at 1.34 ppm (^{1}H) and 69.6 ppm (^{13}C). Since the Ni-CH$_{alkyl}$ [1]H resonance was buried amongst several the cyclohexyl and adamantyl signals, the chemical shift assignment was dependent on the multiplicity of the alkyl ^{13}C resonance (triplet; $^2J_{CP}$ = 10.5 Hz) and heteronuclear 2D NMR spectral techniques (^{1}H-^{31}P HMBC, ^{1}H-^{13}C HSQC; see SI). For comparison, the Ni-CH$_{alkyl}$ peaks appear at 1.81 ppm and 64.6 ppm in **PCPNiBr**.[13]

X-ray-quality crystals of **1** were obtained from a concentrated pentane solution at room temperature. The solid state structure of **1** shows a slightly distorted square planar geometry at the nickel center (τ_4 = 0.13), with the two largest angles at Ni being 165.48(3)°

a. Department of Chemistry, Rutgers University – Newark, Newark, New Jersey 07102, United States. Email: demyan.prokopchuk@rutgers.edu
b. Canadian Light Source, Saskatoon, Saskatchewan, S7N2V3, Canada.

(∠P1–Ni–P2) and 175.81(8)° (∠C33–Ni–C36). The Ni-Ph ligand is slightly canted, as the angle measured from the centroid of the aryl ring to the Ni-C36 bond axis is 171.0° (Figure 1, left). The aryl ring is almost perpendicular to the plane made by the PCP donor atoms (81.73°), largely due to the steric constraints imposed by the bulky cyclohexyl groups.
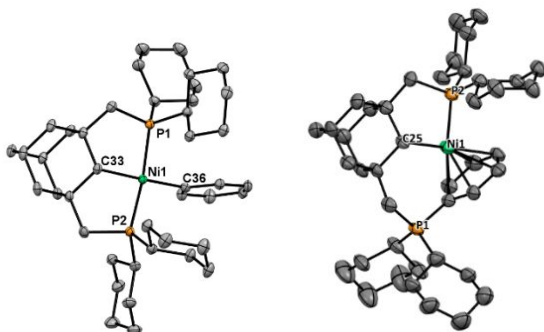

Fig. 1. Molecular structures of **1** (left) and **2** (right) with 50% probability ellipsoids. H atoms, cocrystallized solvent, and B(C_6F_5)$_4$⁻ are omitted for clarity.

Cyclic voltammetry (CV) experiments reveal that **1** has a $Ni^{III/II}$ redox feature at $E_{1/2}$ = -0.14 V vs Fc$^{+/0}$, prompting us to use ferrocenium (Fc⁺) as a chemical oxidant in our attempts to isolate the Ni^{III} radical cation (CVs described later in detail). Surprisingly, reacting **1** with one equiv [Fc][B(C_6F_5)$_4$][14] yields unreacted starting material along with the dicationic Ni^{II} complex **[PCP(η⁶-C_6H_5)Ni][B(C_6F_5)$_4$]$_2$** (**2**) whose structure was unambiguously determined by single crystal X-ray diffraction (Figure 1, right). This unusual complex can be viewed as a phosphine insertion product, where the aryl ligand migrates to phosphorus to generate an arylphosphonium "arm" that coordinates to the cationic Ni^{II} center as an η⁶-arene ligand. Consequently, one phosphorus atom becomes disconnected from the nickel centre while the other phosphine moiety retains its original Ni-P bond.

Complete consumption of **1** is achieved after stirring overnight with 2 equiv of [Fc][B(C_6F_5)$_4$] at room temperature, affording brown-yellow **2** in 44% yield after workup and crystallization (Scheme 1). Two singlets are observed at 94.2 and 20.4 ppm by ^{31}P NMR spectroscopy, with the latter corresponding to the phosphonium cation based on heteronuclear 2D NMR spectroscopic analysis and literature precedent.[15] Compared to complex **1**, dicationic **2** contains deshielded resonances for the coordinated phosphine (94.2 ppm) and Ni-CH$_{alkyl}$ proton (3.13 ppm). The large $^1J_{PC}$ values for the carbon atoms attached to the phosphonium moiety (67.5, 35.9, 36.8 Hz) are typical for phosphonium salts.[16, 17] When **2** is reduced with 2 equiv of bis(pentamethylcyclopentadienyl)chromium (Cp*$_2$Cr; $E_{1/2}$ = -1.47 V vs. Fc$^{+/0}$, THF), complex **1** is regenerated in 90% yield, as determined by inverse-gated ^{31}P NMR spectroscopy on a crude reaction mixture (Figure S10). In situ oxidation of **1** with 2 equiv of [Fc][B(C_6F_5)$_4$] and sequential reduction with 2 equiv of Cp*$_2$Cr results in a 98% recovery of **1** (see SI for details). Therefore, these oxidation and reduction reactions demonstrate that the addition or removal of electrons triggers bond reorganizations involving the arene, phosphine, and nickel moieties.

Cyclic voltammograms (CVs) of **1** were conducted under N_2 in THF to investigate the redox behaviour of **1** and obtain mechanistic insights into the formation of **2**. Narrowing the scan window to only include the redox couple centred at -0.14 V shows higher scan rates increase reversibility (Fig 2, Table S1). Furthermore, comparison of the peak-to-peak separation of this redox couple (ΔE = 77 mV) to the redox peak of Cp*$_2$Fe (ΔE = 81mV) indicates that it is a 1e⁻ redox process (Figure S12, Table S2). We assign this to be the $Ni^{III/II}$ redox couple ($E_{1/2}$ = -0.14 V), which is about 0.2 V more negative than for **PCPNiBr** ($E_{1/2}$ = 0.16 V).
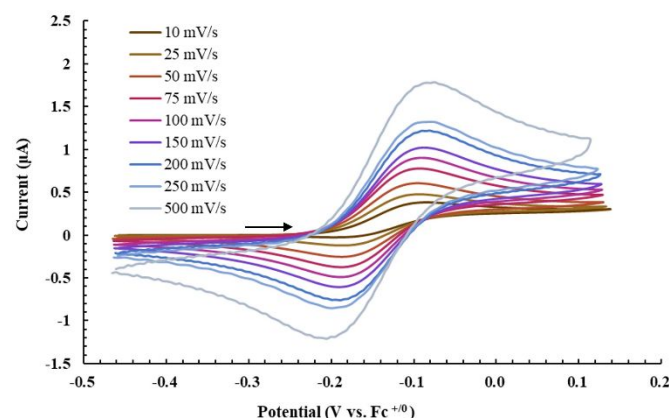

Fig. 2. *iR*-compensated cyclic voltammograms of the $Ni^{III/II}$ redox couple for **1** at different scan rates. Conditions: N_2, THF, 1 mM analyte, 0.1 M [$^nBu_4N$][PF$_6$], PEEK-encased glassy carbon working electrode, Type 2 glassy carbon rod counter electrode, Ag/AgCl pseudoreference electrode. Initial scan direction and starting position indicated with a black arrow.

Gratifyingly, the redox-active Ni^{III} cation [**PCPNiPh**]•⁺ (**1**•⁺) was characterized via EPR spectroscopy by oxidizing **1** at -78 °C with one equiv [Fc][B(C_6F_5)$_4$] in 2-MeTHF. The solution immediately changes from yellow to deep blue-green and X-band EPR spectroscopic analysis at 77 K reveals an axial spectrum which is modelled as an S = 1/2 system ($g_\parallel$ = 2.295, $g_\perp$ = 2.053) with anisotropic hyperfine coupling to two inequivalent P nuclei ($A(^{31}P_1)$ = ± [61, 75] MHz, $A(^{31}P_2)$ = ± [51, 78] MHz; Fig 3, left). DFT calculations show that most of the unpaired spin density resides at the metal centre, while the remainder is distributed onto the alkyl and aryl carbons bonded to nickel (Fig 3, right).
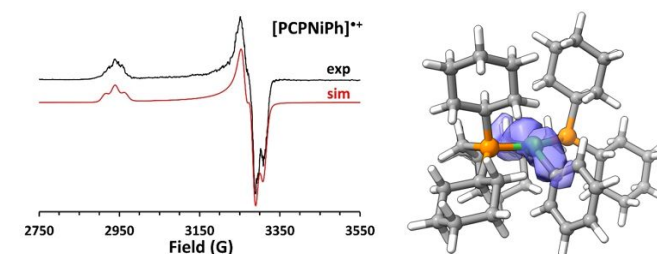

Fig. 3. Left: Experimental (black) and simulated (red, offset) X-band EPR spectra of **1**•⁺ (77 K, 2-MeTHF glass). Right: Computed residual spin density of **1**•⁺ (blue; isosurface value = 0.003) at the TPSS-D3(BJ)/def2-TZVP level of theory.

COMMUNICATION

A wide CV scan window reveals a pseudo-reversible redox couple centered at -0.14 V vs. Fc⁺/⁰, an irreversible oxidation peak at +0.28 V, and an irreversible reduction peak at -1.31 V (Figure 4A, red). The second oxidation peak at E_{pa} = +0.28 V is therefore proposed to be a 1e⁻ oxidation to generate a highly reactive Ni^{IV} dication. Interestingly, when the scan window is narrowed to exclude the putative $Ni^{III/IV}$ oxidation event, the reduction wave at $E_{pc} \cong$ -1.31 V decreases significantly in current at 100 mV/s (Figure 4A, grey) and is nearly absent at 1000 mV/s (Figure 4C, blue). The same reduction wave at E_{pc} = -1.31 V re-emerges at 1000 mV/s when the scan window is opened to include the $Ni^{III/IV}$ oxidation event (Figure 4C, purple). We propose that oxidation of **1** generates phosphine insertion product **2** in the electrical double layer; however, its rate of formation is gated by the degree of oxidation at nickel (i.e., Ni^{III} vs. Ni^{IV}), suggesting that **2** can be generated via two distinct mechanistic pathways, both which will be described later.

Similar CVs were performed using complex **2** but voltages were first swept in cathodic direction (Figure 4B). The same cathodic reduction feature exists as for **1**, however two closely spaced features are visible. The cathodic peak potential with has a maximum peak current (I_{pc} = -1.8 μA) that is twice the intensity of the $Ni^{II/III}$ oxidation (I_{pa} = 0.9 μA), suggesting that **2** undergoes a 2e⁻ reduction to generate a Ni^0 intermediate prior to ligand reorganization (Fig 4B, orange). Overall, the same $Ni^{II/III}$ and $Ni^{III/IV}$ features present in **1** are observed, indicating the clean formation of **1** upon reduction of **2**. Therefore, the analogous electrochemical traces for both complexes on these CV timescales highlight the facile ligand insertion/elimination chemistry mediated by nickel.
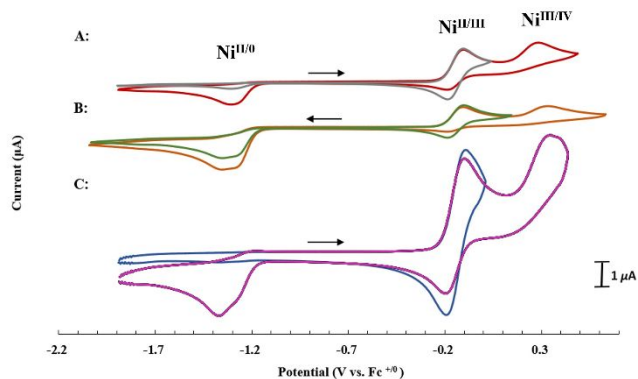

Fig. 4. **A**: *i*R-compensated cyclic voltammograms of **1** at 100 mV/s with wider (red) and narrower (grey) scan windows. **B**: *i*R-compensated cyclic voltammograms of **2** at 100 mV/s with wider (orange) and narrower (green) scan windows.. **C**: *i*R-compensated cyclic voltammograms of **1** at 1000 mV/s with wider (purple) and narrower (blue) scan windows. Conditions: N₂, THF, 1 mM analyte, 0.1 M [ⁿBu₄N][PF₆], PEEK-encased glassy carbon working electrode, Type 2 glassy carbon rod counter electrode, Ag/AgCl pseudoreference electrode. Initial scan direction and starting position indicated with a black arrow. All CV traces are shown for the third scan of each experiment.

Mechanisms for these redox-triggered processes are proposed based on the above CV measurements and corroborated with ground-state DFT calculations using ORCA 5.0.3.[18] A multi-level approach was used where the DFT-optimized structures at a lower level of theory (TPSS-D3(BJ)/def2-TZVP) were used in single point energy calculations with

the larger def2-QZVPP basis set[19, 20] and the PW6B95-D3(BJ) functional (see SI).[21] This functional was chosen for its good performance in the GMTKN55,[22] MOR41,[23] and ROST61[24] benchmark databases. After 1e⁻ oxidation of **1** to generate complex **1•⁺**, two routes are conceivable for the generation of **2**. First, oxidizing conditions strong enough to form a Ni^{IV} complex (**A**) would trigger rapid reductive elimination to afford **2**. Computations reveal that **A** is a strongly oxidizing 14e⁻ Ni^{IV} dication that undergoes rapid reductive elimination ($\Delta G^{\ddagger}$ = 2.8 kcal/mol) to irreversibly generate **2** ($\Delta G_{A \to 2}$ = -37.2 kcal/mol), consistent with our CV data in Fig 4.

The second route, which is traversed in the presence of Fc⁺, involves a slower reductive elimination process via **1•⁺** to generate an (η⁶-arene)Ni^I cation (**B**). This route is computed to be thermodynamically uphill ($\Delta G_{1 \bullet^+ \to B}$ = 7.4 kcal/mol) with a high transition state free energy barrier ($\Delta G^{\ddagger}$ = 26.2 kcal/mol). Although the TS barrier has likely been overestimated for this slow elementary step,[25] the mean average deviation for open-shell organometallics is known to be 2.5 kcal/mol at the applied level of theory.[24] Notwithstanding, the EPR and CV data described earlier clearly indicate that the buildup of **1•⁺** occurs in solution prior to the slow formation of **2**. This step is analogous to the proposed reductive elimination step during nickel-catalyzed arylphosphonium production, however the phosphonium product in unable to fully dissociate from the metal centre in the case of **B**. Finally, strongly reducing **B** ($E°_{DFT}$ = -0.94 V) is easily oxidized by exogenous Fc⁺ to generate **2**.
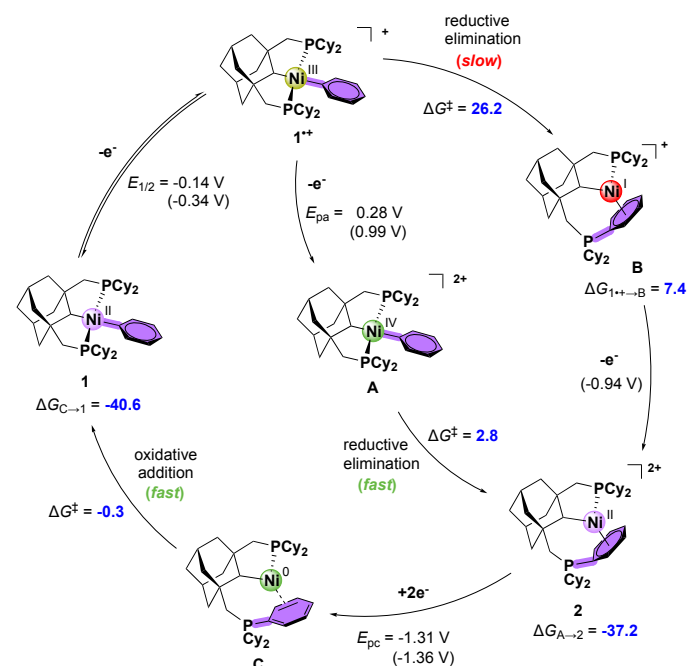
Scheme 2. Proposed mechanism describing two different pathways of generating **2** from **1** via 2e⁻ oxidation and the regeneration of **1** from **2** via 2e⁻ reduction. Redox potentials are given in Volts vs. Fc⁺/⁰, DFT-computed redox potentials are shown in parentheses, and computed free energies (blue) are shown in kcal/mol.

Consistent with the above CV data, the formation of **1** starting from **2** is proposed to follow a different mechanistic pathway, where 2e⁻ reduction forms a putative Ni^0 complex (**C**). Experiment reveals two

COMMUNICATION   Journal Name

closely spaced reductions centered at $E_{pc} \cong$ -1.31 V (Fig 4), and DFT calculations modelling a 2e$^-$ Ni$^{II/0}$ redox process are in excellent agreement ($E°_{DFT}$ = -1.36 V). Finally, a very rapid oxidative addition involving P-C bond cleavage furnishes **1**, which is computed to be barrierless ($\Delta G^{\ddagger}$ = -0.3 kcal/mol) and very exothermic ($\Delta G_{C \rightarrow 1}$ = -40.6 kcal/mol). The oxidative addition of phosphonium salts to Pd^0 has been observed during aryl-aryl interchange between phosphine ligands,[26] however to the best of our knowledge, this type of reactivity has not been previously documented at Ni^0. Notably, the oxidative addition of an η^6-arylphosphonium moiety at Ni^0 suggests that pre-coordination of the arene is crucial in the mechanism of Ni-catalyzed reductive cross coupling using arylphosphonium substrates.[27]

In summary, we report the synthesis of two new aryl-containing nickel complexes, and their electrochemically mediated interconversion represents an unprecedented example of reversible aryl insertion into a metal-phosphine bond. Based on electrochemical measurements, EPR spectroscopy, and DFT calculations, a mechanism is proposed where the PCP ligand acts as a chemically non-innocent moiety with the metal accommodating formal oxidation states from Ni^0 to Ni^{IV}. The reductive elimination step via Ni^{III} represents a glimpse into the mechanism of arylphosphonium salt synthesis, suggesting that an η^6-arene intermediate may be formed prior to product dissociation.

Conflicts of interest

There are no conflicts to declare.

Notes and references

1. D. W. Allen and P. E. Cropper, *J. Organomet. Chem.*, 1992, **435**, 203.
2. D. Marcoux and A. B. Charette, *J. Org. Chem.*, 2008, **73**, 590.
3. D. Marcoux and A. B. Charette, *Adv. Synth. Catal.*, 2008, **350**, 2967.
4. T. Migita, T. Nagai, K. Kiuchi and M. Kosugi, *Bull. Chem. Soc. Jpn.*, 1983, **56**, 2869.
5. T. Migita, T. Shimizu, Y. Asami, J.-i. Shiobara, Y. Kato and M. Kosugi, *Bull. Chem. Soc. Jpn.*, 1980, **53**, 1385.
6. T. T. Tsou and J. K. Kochi, *J. Am. Chem. Soc.*, 1979, **101**, 7547.
7. O. R. Luca, J. D. Blakemore, S. J. Konezny, J. M. Praetorius, T. J. Schmeier, G. B. Hunsinger, V. S. Batista, G. W. Brudvig, N. Hazari and R. H. Crabtree, *Inorg. Chem.*, 2012, **51**, 8704.
8. A. Castonguay, D. M. Spasyuk, N. Madern, A. L. Beauchamp and D. Zargarian, *Organometallics*, 2009, **28**, 2134.
9. B. Vabre, P. Petiot, R. Declercq and D. Zargarian, *Organometallics*, 2014, **33**, 5173.
10. R. Gerber, O. Blacque and C. M. Frech, *ChemCatChem*, 2009, **1**, 393.
11. R. Gerber, O. Blacque and C. M. Frech, *Dalton Trans.*, 2011, **40**, 8996.
12. R. Gerber, T. Fox and C. M. Frech, *Chem. Eur. J.*, 2010, **16**, 6771.
13. L. Lin, D. M. Spasyuk, R. A. Lalancette and D. E. Prokopchuk, *J Am Chem Soc*, 2022, **144**, 12632.
14. H. A. Spinney, C. R. Clough and C. C. Cummins, *Dalton Trans*, 2015, **44**, 6784.
15. X. F. Zhu, C. E. Henry and O. Kwon, *J Am Chem Soc*, 2007, **129**, 6722.
16. C. Reitsamer, S. Stallinger, W. Schuh, H. Kopacka, K. Wurst, D. Obendorf and P. Peringer, *Dalton Trans*, 2012, **41**, 3503.
17. C. Puke, G. Erker, B. Wibbeling and R. Fröhlich, *Eur. J. Org. Chem.*, 1999, 1831.
18. F. Neese, *WIREs Comput. Mol. Sci.*, 2022, **12**, e1606.
19. F. Weigend and R. Ahlrichs, *Phys. Chem. Chem. Phys.*, 2005, **7**, 3297.
20. F. Weigend, *Phys. Chem. Chem. Phys.*, 2006, **8**, 1057.
21. Y. Zhao and D. G. Truhlar, *J. Phys. Chem. A*, 2005, **109**, 5656.
22. L. Goerigk, A. Hansen, C. Bauer, S. Ehrlich, A. Najibi and S. Grimme, *Phys. Chem. Chem. Phys.*, 2017, **19**, 32184.
23. S. Dohm, A. Hansen, M. Steinmetz, S. Grimme and M. P. Checinski, *J. Chem. Theory Comput.*, 2018, **14**, 2596.
24. L. R. Maurer, M. Bursch, S. Grimme and A. Hansen, *J. Chem. Theory Comput.*, 2021, **17**, 6134.
25. Assuming that this intramolecular oxidative addition reaction is independent of the initial concentration of 1, we estimate that that half-life is about 10 min since the reaction is complete in 1 h via NMR reaction monitoring (to 6 half-lives). Thus, the rate constant k is approximately 1 x 10^{-3} s^{-1}, translating to a maximum free energy barrier of 22 kcal/mol using classical transition state theory.
26. F. E. Goodson, T. I. Wallow and B. M. Novak, *J. Am. Chem. Soc.*, 1997, **119**, 12441.
27. H. Wang, M. Yang, Y. Wang, X. Man, X. Lu, Z. Mou, Y. Luo and H. Liang, *Org. Lett.*, 2021, **23**, 8183.